The Canadian Mineralogist
Vol. 56, pp. 811-820 (2018)
DOI: 10.3749/canmin.1800044

PARARAISAITE, THE DIMORPH OF RAISAITE, FROM THE NORTH STAR MINE, TINTIC, UTAH, USA

ANTHONY R. KAMPF[§]

Mineral Sciences Department, Natural History Museum of Los Angeles County, 900 Exposition Boulevard, Los Angeles, California 90007, USA

ROBERT M. HOUSLEY AND GEORGE R. ROSSMAN

Division of Geological and Planetary Sciences, California Institute of Technology, Pasadena, California 91125, USA

ABSTRACT

Pararaisaite, $Cu^{2+}Mg[Te^{6+}O_4(OH)_2]\cdot 6H_2O$, is a new mineral from the North Star mine, Tintic district, Juab County, Utah, USA. It is an oxidation-zone mineral occuring in vugs in a matrix of massive quartz with embedded crystals of baryte and goldfieldite. Crystals are deep blue, striated prisms up to 0.4 mm in length, elongated on [010] and exhibiting the forms {100}, {001}, {102}, {102}, and {114}. The mineral is transparent with vitreous luster, white streak, Mohs hardness 2½, brittle tenacity, splintery fracture, and two cleavages: perfect on {001} and good on {100}. The measured density is 2.85(2) g/cm^3. Pararaisaite is biaxial (+) with $\alpha = 1.600(2)$, $\beta = 1.616(2)$, $\gamma = 1.713(3)$ (white light); $2V = 47(1)°$; slight $r > v$ dispersion; orientation $Z = \mathbf{b}$, $X \approx \mathbf{a}$, $Y \approx \mathbf{c}$; and pleochroism X very pale purple, Y purple, Z blue green ($X << Z < Y$). The Raman spectrum is consistent with the presence of tellurate, OH, and H_2O. Electron-microprobe analyses gave the empirical formula $(Mg_{1.10}Cu_{0.93}Te_{0.96}Sb_{0.01})_{\Sigma 3}O_{12}H_{14.12}$. The mineral is monoclinic, space group $P2_1/c$, with a 9.6838(5), b 5.75175(19), c 17.6339(12) Å, β 90.553(6)°, V 982.14(9) Å^3, and $Z = 4$. The five strongest X-ray powder diffraction lines are [d_{obs} Å(I)(hkl)]: 8.77(100)(002), 4.824(71)(200,111), 4.248(85)($\bar{2}$02, 202), 2.419(50)(400,024), and 1.8929(48)($\bar{2}$26, 226). Pararaisaite is dimorphous with raisaite. The structure contains straight edge-sharing chains of alternating $Cu^{2+}O_4(OH)_2$ and $Te^{6+}O_4(OH)_2$ octahedra. The chains link to one another *via* shared octahedral corners to form $[Cu^{2+}Te^{6+}O_4(OH)_2]^{2-}$ sheets. Interlayer $Mg(H_2O)_6$ octahedra link the sheets *via* hydrogen bonds.

Keywords: pararaisaite, raisaite, new mineral, tellurium oxysalt, crystal structure, Raman spectroscopy, electron microprobe analysis, North Star mine, Tintic, Utah, USA.

INTRODUCTION

In their structural classification of tellurium oxysalts, Christy *et al*. (2016) noted the remarkable diversity of mineral species containing Te as an essential constitutent. Tellurium occurs in oxysalts as both the Te^{4+} (tellurite) and Te^{6+} (tellurate) cation, both of which combine with a variety of other cations and anions and exhibit a wide variety of polymerizations. Te^{4+} has a stereoactive lone-electron pair and typically strongly bonds to three O atoms to form the pyramidal $(Te^{4+}O_3)^{2-}$ group, while Te^{6+} is almost always octahedrally coordinated by O. Although the structures of Te oxysalts are generally assembled from the same structural components, most Te-oxysalt minerals exhibit unique structural motifs.

In nature, Te oxysalts most commonly occur in the oxidation zones of epithermal Au-Te and base-metal deposits, where the Te^{4+} and Te^{6+} atoms often combine with other cations such as Pb^{2+}, Cu^{2+}, and Zn^{2+}. Structures combining Te^{6+} and Cu^{2+} are particularly interesting because of the different polymerization possibilities engendered by the strongly bonded and very regular $Te^{6+}O_6$ octahedra and Jahn-Teller distorted $Cu^{2+}O_6$ octahedra (also $Cu^{2+}O_5$ square pyramids and $Cu^{2+}O_4$ square-planar groups). Including pararaisaite, there are 25 known

§ *Corresponding author e-mail address*: akampf@nhm.org

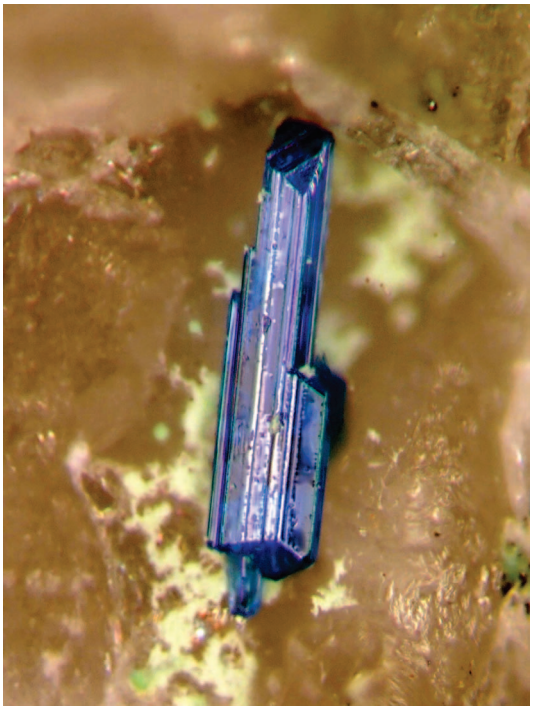

FIG. 1. Pararaisaite on quartz; FOV 0.45 mm.

minerals containing both Te^{6+} and Cu^{2+} as essential constituents. Although the structures of several have not been determined, all known structures are unique among minerals. Furthermore, although timroseite, $Pb_2Cu^{2+}{}_5(Te^{6+}O_6)_2(OH)_2$, and paratimroseite, $Pb_2Cu^{2+}{}_4(Te^{6+}O_6)_2(H_2O)_2$, are closely related compositionally and structurally (Kampf *et al*. 2010), until now, no minerals containing both Te^{6+} and Cu^{2+} as essential constituents have exhibited dimorphism. Herein, we describe the new mineral pararaisaite, which is dimorphous with raisaite, $Cu^{2+}Mg[Te^{6+}O_4(OH)_2]\cdot 6H_2O$ (Pekov *et al*. 2016). It is also noteworthy that only one example of dimorphism exists among minerals containing both Te^{4+} and Cu^{2+} as essential constituents: millsite and teinite are dimorphs of $Cu[Te^{4+}O_3]\cdot 2H_2O$ (Rumsey *et al*. 2018).

The mineral name pararaisaite (/ pær ə rɑ: 'i: sɑ: aɪt /) is from the Greek "para" for near and for the mineral's relation to raisaite. The new mineral and name have been approved by the Commission on New Minerals, Nomenclature and Classification of the International Mineralogical Association (IMA2017-110). The holotype specimen is housed in the collections of the Mineral Sciences Department, Natural History Museum of Los Angeles County, 900 Exposition Boulevard, Los Angeles, California 90007, USA, catalogue number 67272.

Occurrence and Paragenesis

Pararaisaite occurs in the North Star mine, Mammoth, Tintic district, Juab County, Utah, USA (39°55′14″N 112°6′28″W). The North Star mine exploited a polymetallic (Au-Ag-Cu-Pb) vein deposit emplaced in contact-metamorphosed dolomite and was the largest producer of gold in the Tintic district. The North Star mine was discovered in 1885, closed in 1900, and reported to be inaccessible as of 1911. The principle ore minerals were galena, cerussite, and enargite and the prominent gangue minerals were quartz and baryte (Lindgren & Loughlin 1919). A wide variety of oxidation-zone minerals have been collected from the mine dumps by collectors.

Pararaisaite is an oxidation-zone mineral known from only three crystals on the holotype specimen and a few small broken crystals on two other small specimens. It occurs in vugs in a matrix of massive quartz with embedded crystals of baryte and goldfieldite. The only associated secondary mineral is malachite, which occurs as crusts and cavity fillings. The holotype specimen was collected and provided for study by Charles Adan of Salt Lake City, Utah (USA).

Physical and Optical Properties

Pararaisaite occurs as deep blue, striated, prismatic crystals up to 0.4 mm in length (Figs. 1 and 2). The prisms are elongate on [010] and exhibit the forms {100}, {001}, {102}, {10$\bar{2}$}, and {114}. No twinning was observed. The streak is white, the luster is vitreous, and crystals are transparent. The mineral is nonfluorescent under long- and short-wave ultraviolet light. The Mohs hardness is 2½ based on scratch tests. The tenacity is brittle, the cleavage is perfect on {001} and good on {100}, and the fracture is splintery. The density measured by flotation in a mixture of methylene iodide and toluene is 2.85(2) g/cm^3. The calculated density is 2.812 g/cm^3 for the empirical formula and 2.851 g/cm^3 for the ideal formula. In dilute or concentrated HCl at room temperature, the crystals lose color immediately and birefringence slowly, but do not dissolve.

Optically, the mineral is biaxial positive with indices of refraction $\alpha = 1.600(2)$, $\beta = 1.616(2)$, and $\gamma = 1.713(3)$ measured in white light. The $2V$ determined by direct measurement on a spindle stage is 47(1)°; the calculated $2V$ is 46.3°. Slight $r > v$ dispersion of the optic axes was observed. The optical orientation is $Z = \mathbf{b}$, $X \approx \mathbf{a}$, $Y \approx \mathbf{c}$ and the pleochroism is X very pale purple, Y purple, Z blue green; $X << Z < Y$. The Gladstone-Dale compatibility $1 - (K_p/K_c)$

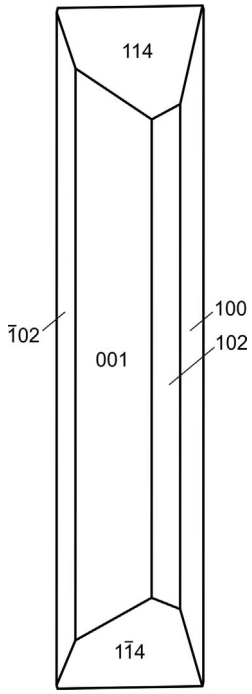

FIG. 2. Crystal drawing of pararaisaite; clinographic projection in non-standard orientation, **b** vertical.

(Mandarino 1976) is –0.012 (superior) based on the empirical formula and –0.005 (superior) based on the ideal formula.

RAMAN SPECTROSCOPY

Raman spectra were recorded using a Renishaw M1000 micro-Raman spectrometer system. Light from a 514.5 nm solid-state laser was focused through an Olympus microscope onto the samples with a 100× objective lens resulting in an incident spot size of about 1 μm in diameter. To avoid any possible sample damage, the laser was run at only 10% power (~2 mW at the sample) for the measurements reported. Peak positions were periodically calibrated against a silicon (520.5 cm^{-1}) standard and generally varied less than 0.3 cm^{-1}. All spectra were obtained with a dual-wedge polarization scrambler inserted directly above the objective lens to minimize the effects of polarization. The spectrum from 4000 to 100 cm^{-1} is shown in Figure 3.

The sharp, intense bands confirm the good crystallinity of the sample. Bands in the 3600–3000 cm^{-1} range correspond to O–H stretching vibrations of OH and H_2O groups. The strongest bands occur at 708, 682, 573, and 526 cm^{-1}; tellurate groups, $Te^{6+}O_6$, have previously been shown to have strong bands in the 800–600 cm^{-1} region (*cf.* Blasse & Hordijk 1972, Kampf *et al*. 2013, Frikha *et al*. 2017). The 708 and 682 cm^{-1} bands likely correspond to the tellurate stretching vibration modes, and the 573 and 526 cm^{-1} bands can be assigned to the tellurate bending vibration modes. Other features occur at 1117, 1049, 405, 389, 337, 246, 225, and 183 cm^{-1}.

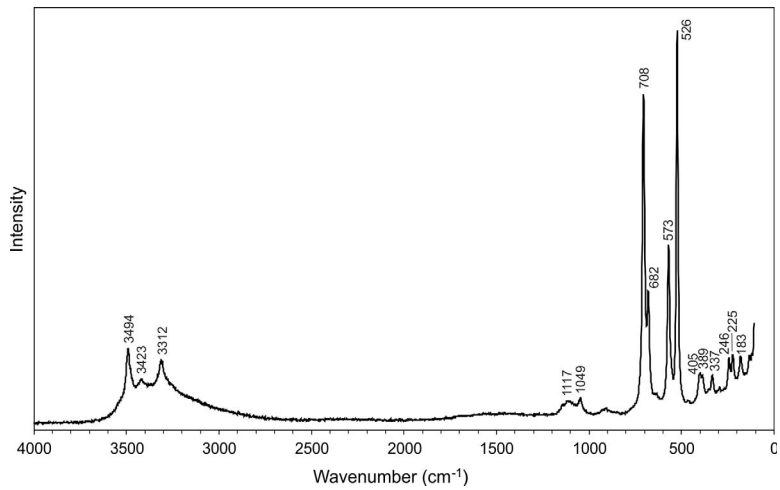

FIG. 3. The Raman spectrum of pararaisaite recorded with a 514 nm laser.

TABLE 1. ANALYTICAL DATA (wt.%) FOR PARARAISAITE

Constituent	Mean	Range	SD	Standard
MgO	11.14	10.78–11.50	0.33	syn. forsterite
CuO	18.59	18.35–18.80	0.21	Cu metal
Sb_2O_5	0.26	0.20–0.32	0.05	syn. GaAs
TeO_3	42.55	42.20–43.21	0.46	Te metal
H_2O*	31.97			
Total	104.51			

* Based on the crystal structure.

Chemical Composition

Four chemical compositions were obtained from one crystal using a JEOL 8200 electron microprobe in WDS mode. The voltage was maintained at 15 kV and a 5 μm beam diameter was used for all analyses. The crystal was very sensitive to damage from the beam. A 15 nA beam current was initially used; this was reduced to 5 nA and then to 1 nA, but all analyses yielded similar results. No other elements were detected by EDS. Because insufficient material is available for a direct determination of H_2O, it was calculated based upon the structure determination. The loss of weakly held H_2O under vacuum and/or during analyses accounts for the high EPMA totals when calculated H_2O is included. Analytical data are given in Table 1. The empirical

TABLE 2. POWDER DATA FOR PARARAISAITE (ONLY CALCULATED LINES WITH $I \geq 2$ ARE INCLUDED)

I_{obs}	d_{obs}	d_{calc}	I_{calc}	$h\,k\,l$	I_{obs}	d_{obs}	d_{calc}	I_{calc}	$h\,k\,l$
100	8.77	8.8165	100	0 0 2	13	2.0568	2.0555	8	0 2 6
		4.8417	32	2 0 0	4	2.0109	2.0134	2	$\bar{2}$ 0 8
71	4.824	4.7676	2	$\bar{1}$ 1 1	48	1.8929	1.8966	13	$\bar{2}$ 2 6
		4.7554	20	1 1 1			1.8874	13	2 2 6
43	4.392	4.4083	42	0 0 4			1.8698	2	1 3 1
85	4.248	4.2612	39	$\bar{2}$ 0 2	11	1.8578	1.8597	2	4 0 6
		4.2267	38	2 0 2			1.8520	4	4 2 0
16	3.792	3.7933	11	$\bar{1}$ 1 3			1.8238	3	5 1 1
26	3.263	3.2754	10	$\bar{2}$ 0 4	21	1.8150	1.8152	3	$\bar{4}$ 2 2
		3.2440	10	2 0 4			1.8098	3	4 2 2
13	2.930	2.9388	11	0 0 6			1.7633	3	0 0 10
11	2.860	2.8759	3	0 2 0	29	1.7530	1.7566	2	$\bar{5}$ 1 3
		2.8646	4	1 1 5			1.7494	12	0 2 8
39	2.733	2.7341	17	0 2 2	24	1.7101	1.7120	8	$\bar{4}$ 2 4
5	2.533	2.5319	2	$\bar{1}$ 1 6			1.7030	8	4 2 4
9	2.483	2.4726	6	2 2 0			1.6620	2	$\bar{2}$ 0 10
50	2.419	2.4208	17	4 0 0	19	1.6501	1.6517	2	2 0 10
		2.4086	30	0 2 4			1.6494	3	$\bar{2}$ 2 8
27	2.387	2.3838	5	$\bar{2}$ 2 2			1.6413	3	2 2 8
		2.3777	5	2 2 2			1.6377	2	$\bar{4}$ 0 8
18	2.339	2.3402	7	$\bar{4}$ 0 2	15	1.6245	1.6220	3	4 0 8
		2.3287	8	4 0 2			1.6139	3	6 0 0
5	2.258	2.2491	3	$\bar{1}$ 1 7	8	1.5882	1.5902	3	$\bar{6}$ 0 2
4	2.202	2.2041	3	0 0 8			1.5848	4	6 0 2
14	2.157	2.1611	5	$\bar{2}$ 2 4	10	1.5675	1.5721	4	$\bar{4}$ 2 6
		2.1520	4	2 2 4			1.5617	4	4 2 6
11	2.124	2.1306	5	$\bar{4}$ 0 4	8	1.5052	1.5032	3	0 2 10
		2.1133	5	4 0 4	3	1.4678	1.4694	3	0 0 12

TABLE 3. DATA COLLECTION AND STRUCTURE REFINEMENT DETAILS FOR PARARAISAITE

Diffractometer	Rigaku R-Axis Rapid II
X-ray radiation / power	Mo$K\alpha$ ($\lambda = 0.71075$ Å)/50 kV, 40 mA
Temperature	298(2) K
Structural Formula	$(Cu_{0.94}Mg_{0.06})Mg[(Te_{0.98}Mg_{0.02})O_4(OH)_2]\cdot 6H_2O$
Space group	$P2_1/c$
Unit cell dimensions	$a = 9.6838(5)$ Å $b = 5.75175(19)$ Å $c = 17.6339(12)$ Å $\beta = 90.553(6)°$
V	982.14(9) Å^3
Z	4
Density (for above formula)	2.820 g·cm^{-3}
Absorption coefficient	5.082 mm^{-1}
F(000)	805
Crystal size	220 × 35 × 20 μm
θ range	3.11 to 25.02°
Index ranges	$-11 \le h \le 11$, $-6 \le k \le 6$, $-20 \le l \le 20$
Refls collected / unique	8155 / 1685; $R_{int} = 0.036$
Reflections with $I_o > 2\sigma I$	1435
Completeness to $\theta = 25.02°$	97.20%
Refinement method	Full-matrix least-squares on F^2
Parameters / restraints	183 / 20
GoF	1.116
Final R indices [$I_o > 2\sigma I$]	$R_1 = 0.0207$, $wR_2 = 0.0467$
R indices (all data)	$R_1 = 0.0259$, $wR_2 = 0.0485$
Largest diff. peak / hole	+1.04 / –0.39 e/A^3

*$R_{int} = \Sigma|F_o^2 - F_o^2(\text{mean})|/\Sigma[F_o^2]$. GoF = $S = \{\Sigma[w(F_o^2 - F_c^2)^2]/(n-p)\}^{1/2}$. $R_1 = \Sigma||F_o| - |F_c||/\Sigma|F_o|$. $wR_2 = \{\Sigma[w(F_o^2 - F_c^2)^2]/\Sigma[w(F_o^2)^2]\}^{1/2}$; $w = 1/[\sigma^2(F_o^2) + (aP)^2 + bP]$ where a is 0.0212, b is 0, and P is $[2F_c^2 + \text{Max}(F_o^2, 0)]/3$.

formula (based on 12 O atoms per formula unit, *apfu*) is $(Mg_{1.10}Cu^{2+}_{0.93}Te^{6+}_{0.96}Sb^{5+}_{0.01})_{\Sigma 3}O_{12}H_{14.12}$. The simplified formula is $Cu^{2+}Mg[Te^{6+}O_4(OH)_2]\cdot 6H_2O$, which requires MgO 9.56, CuO 18.87, TeO_3 41.65, H_2O 29.91, total 100.00 wt.%.

X-Ray Crystallography

Powder X-ray studies were done using a Rigaku R-Axis Rapid II curved imaging plate microdiffractometer with monochromatized Mo$K\alpha$ radiation ($\lambda = 0.71075$ Å). A Gandolfi-like motion on the φ and ω axes was used to randomize the samples. Observed d values and intensities were derived by profile fitting using JADE 2010 software. Data are given in Table 2. Unit-cell parameters refined from the powder data using JADE 2010 with whole pattern fitting are a 9.720(2), b 5.757(2), c 17.624(2) Å, β 90.549(4)°, and V 986.2(4) Å^3.

Single-crystal data were collected using the same diffractometer and radiation as noted above. The Rigaku CrystalClear software package was used for processing the structure data, including the application of an empirical absorption correction using the multi-scan method with ABSCOR (Higashi 2001). The structure was solved by the charge-flipping method using SHELXT (Sheldrick 2015a). Refinement proceeded by full-matrix least-squares on F^2 using SHELXL-2016 (Sheldrick 2015b). The two Mg sites (Mg1 and Mg2) were assigned full occupancy by Mg. The Cu site was refined with joint occupancy by Cu and Mg, yielding $Cu_{0.94}Mg_{0.06}$, and the Te site was refined with joint occupancy by Te and Mg, yielding $Te_{0.98}Mg_{0.02}$. The resulting totals for these cations ($Mg_{1.08}Cu_{0.94}Te_{0.98}$) are very close to those in the empirical formula ($Mg_{1.10}Cu_{0.93}Te_{0.96}$). During the final stages of refinement, difference-Fourier syntheses located all H atom positions, which were then refined with soft restraints of 0.82(3) Å on the O–H distances and 1.30(3) Å on the H–H distances and with the U_{eq} of each OH H site set to 1.5 times that of the donor O atom and each H_2O H site set to 1.2 times that of the donor O atom. Data collection and refinement details

TABLE 4. ATOM COORDINATES AND DISPLACEMENT PARAMETERS (Å^2) FOR PARARAISAITE

	x/a	*y/b*	*z/c*	U_{eq}
Te*	0.25107(2)	0.51711(3)	0.75467(2)	0.00807(9)
Cu*	0.24963(3)	1.01683(5)	0.75423(2)	0.01049(18)
Mg1	0	0.5	0	0.0135(3)
Mg2	0.5	0.5	0.5	0.0135(3)
O1	0.2386(2)	0.7629(3)	0.82643(12)	0.0154(5)
O2	0.2576(2)	0.2720(3)	0.82697(12)	0.0150(5)
O3	0.2527(2)	0.2724(3)	0.68119(12)	0.0140(5)
O4	0.2534(2)	0.7613(3)	0.68093(12)	0.0145(5)
OH1	0.4541(2)	0.5215(3)	0.75699(12)	0.0196(5)
H1	0.476(3)	0.650(4)	0.7666(17)	0.029
OH2	0.0478(2)	0.5133(3)	0.75100(12)	0.0186(5)
H2	0.027(3)	0.384(3)	0.7560(17)	0.028
OW1	0.8134(2)	0.6068(4)	0.03343(12)	0.0232(5)
H1A	0.752(2)	0.641(6)	0.0056(12)	0.028
H1B	0.796(3)	0.648(5)	0.0754(10)	0.028
OW2	0.9083(2)	0.2295(3)	0.93724(12)	0.0212(5)
H2A	0.859(3)	0.242(4)	0.9005(14)	0.025
H2B	0.955(3)	0.118(4)	0.9329(15)	0.025
OW3	0.0110(2)	0.7367(3)	0.90816(12)	0.0194(5)
H3A	0.075(2)	0.749(5)	0.8786(15)	0.023
H3B	0.060(2)	0.735(5)	0.8795(15)	0.023
OW4	0.3124(2)	0.6056(4)	0.46473(12)	0.0227(5)
H4A	0.294(3)	0.658(5)	0.4221(10)	0.027
H4B	0.250(2)	0.635(6)	0.4911(13)	0.027
OW5	0.4089(2)	0.2327(3)	0.56357(11)	0.0198(5)
H5A	0.456(3)	0.117(4)	0.5698(15)	0.024
H5B	0.371(3)	0.250(4)	0.6041(13)	0.024
OW6	0.4908(2)	0.7395(3)	0.59108(12)	0.0191(5)
H6A	0.426(2)	0.740(5)	0.6208(15)	0.023
H6B	0.5601(19)	0.747(5)	0.6181(15)	0.023

	U^{11}	U^{22}	U^{33}	U^{23}	U^{13}	U^{12}
Te	0.01138(14)	0.00517(14)	0.00767(13)	0.00004(6)	0.00012(8)	0.00037(7)
Cu	0.0203(3)	0.0033(3)	0.0079(3)	–0.00011(12)	0.00055(17)	–0.00043(14)
Mg1	0.0147(8)	0.0131(7)	0.0126(8)	–0.0002(5)	0.0007(6)	0.0017(5)
Mg2	0.0145(8)	0.0137(8)	0.0123(8)	0.0004(5)	0.0012(6)	0.0006(5)
O1	0.0265(14)	0.0097(12)	0.0101(11)	–0.0021(7)	–0.0001(9)	0.0000(8)
O2	0.0243(14)	0.0115(11)	0.0092(11)	0.0028(7)	0.0020(9)	0.0000(8)
O3	0.0220(13)	0.0116(12)	0.0085(11)	–0.0004(7)	0.0022(9)	0.0004(8)
O4	0.0221(13)	0.0116(12)	0.0098(12)	–0.0014(7)	0.0011(9)	–0.0017(8)
OH1	0.0130(12)	0.0146(12)	0.0312(14)	0.0023(8)	–0.0013(9)	–0.0001(9)
OH2	0.0117(13)	0.0144(12)	0.0297(14)	–0.0023(8)	0.0011(9)	0.0003(9)
OW1	0.0196(13)	0.0368(13)	0.0132(12)	–0.0011(10)	0.0018(9)	0.0098(10)
OW2	0.0240(15)	0.0215(12)	0.0179(13)	–0.0045(9)	–0.0070(10)	0.0043(9)
OW3	0.0191(14)	0.0266(12)	0.0124(12)	0.0038(9)	0.0012(9)	0.0039(9)
OW4	0.0199(14)	0.0349(13)	0.0135(12)	0.0024(9)	0.0004(9)	0.0089(10)
OW5	0.0243(15)	0.0199(12)	0.0153(12)	0.0032(8)	0.0054(10)	0.0039(9)
OW6	0.0199(14)	0.0242(12)	0.0131(12)	–0.0030(8)	0.0015(9)	–0.0002(9)

* Refined occupancies: Te/Mg = 0.980/0.020(3); Cu/Mg = 0.941/0.059(5).

TABLE 5. SELECTED BOND DISTANCES (Å) AND ANGLES (°) FOR PARARAISAITE

Te–O2	1.9015(19)	Cu–O1	1.9413(19)	Mg1–OW1 (×2)	2.002(2)
Te–O1	1.9018(18)	Cu–O2	1.9503(19)	Mg1–OW2 (×2)	2.1012(19)
Te–O3	1.9134(19)	Cu–O3	1.9547(19)	Mg1–OW3 (×2)	2.118(2)
Te–O4	1.9142(19)	Cu–O4	1.9579(18)	<Mg1–O>	2.074
Te–OH1	1.966(2)	Cu–OH1	2.878(2)		
Te–OH2	1.969(2)	Cu–OH2	2.881(2)	Mg2–OW4 (×2)	2.009(2)
<Te–O>	1.928	<Cu–O_{eq}>	1.951	Mg2–OW5 (×2)	2.1018(19)
		<Cu–O_{ap}>	2.880	Mg2–OW6 (×2)	2.119(2)
				<Mg2–O>	2.077

Hydrogen bonds

D–H	*d*(D–H)	*d*(H···A)	*d*(D···A)	<DHA	A
OW1–H1A	0.793(16)	2.038(17)	2.831(3)	178(3)	OW5
OW1–H1B	0.798(16)	1.859(17)	2.656(3)	175(3)	O2
OW2–H2A	0.806(17)	1.795(17)	2.601(3)	178(3)	O4
OW2–H2B	0.789(16)	2.26(2)	2.986(3)	153(3)	OW3
OW3–H3A	0.806(17)	2.018(16)	2.817(3)	171(3)	O3
OW3–H3B	0.856(16)	1.983(16)	2.830(3)	170(3)	O1
OW4–H4A	0.827(16)	1.824(17)	2.645(3)	172(3)	O1
OW4–H4B	0.783(16)	2.070(17)	2.852(3)	177(4)	OW2
OW5–H5A	0.814(16)	2.23(2)	2.984(3)	154(3)	OW6
OW5–H5B	0.813(16)	1.790(17)	2.589(3)	167(3)	O3
OW6–H6A	0.819(16)	1.994(16)	2.807(3)	172(3)	O4
OW6–H6B	0.820(17)	2.011(16)	2.827(3)	173(3)	O2

TABLE 6. BOND-VALENCE ANALYSIS FOR PARARAISAITE (VALUES ARE EXPRESSED IN VALENCE UNITS)

					Hydrogen bonds		
	Mg1	Mg2	Cu	Te	accepted	donated	Σ
O1			0.49	1.03	0.17, 0.26		1.95
O2			0.48	1.03	0.25, 0.17		1.93
O3			0.47	1.01	0.18, 0.30		1.96
O4			0.47	1.01	0.29, 0.18		1.95
OH1			0.03	0.92			0.95
OH2			0.03	0.92			0.95
OW1	$0.41^{\times 2\downarrow}$					–0.17, –0.25	–0.01
OW2	$0.33^{\times 2\downarrow}$				0.17	–0.29, –0.13	0.08
OW3	$0.32^{\times 2\downarrow}$				0.13	–0.18, –0.17	0.10
OW4		$0.40^{\times 2\downarrow}$				–0.26, –0.17	–0.03
OW5		$0.33^{\times 2\downarrow}$			0.17	–0.13, –0.30	0.07
OW6		$0.32^{\times 2\downarrow}$			0.13	–0.18, –0.17	0.10
Σ	2.12	2.10	1.97	5.92			

Bond valence parameters for Mg^{2+}–O and Cu^{2+}–O are from Gagné & Hawthorne (2015). Those for Te^{6+}–O are from Mills & Christy (2013). Hydrogen-bond strengths are based on O–O bond lengths from Ferraris & Ivaldi (1988).

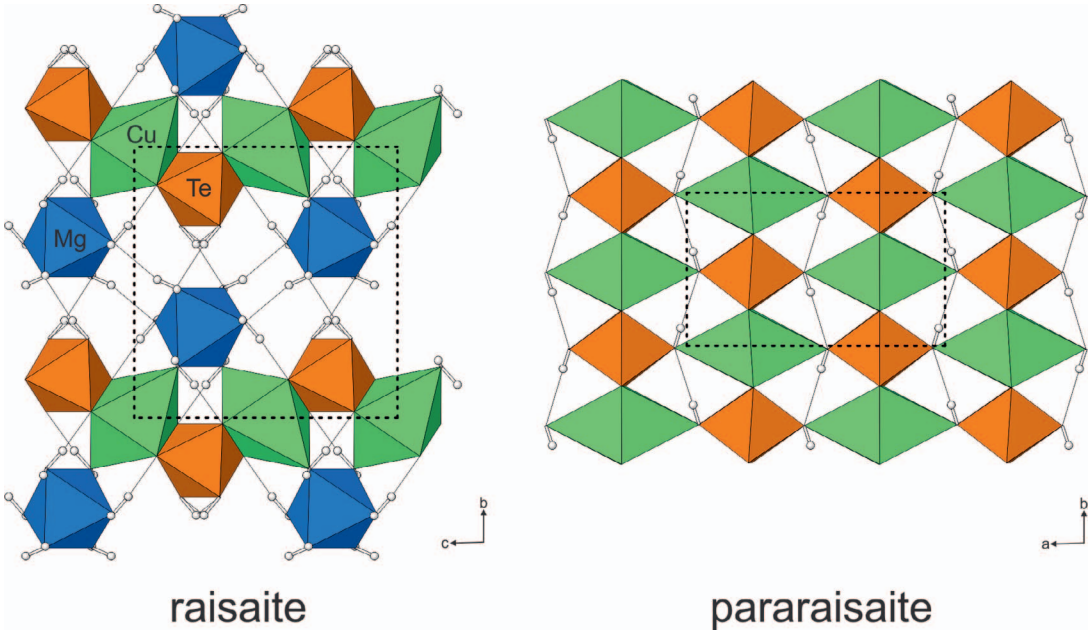

FIG. 4. Layers in the structures of raisaite and pararaisaite. Hydrogen bonds are shown by thin lines. The unit cell outline is shown with dashed lines.

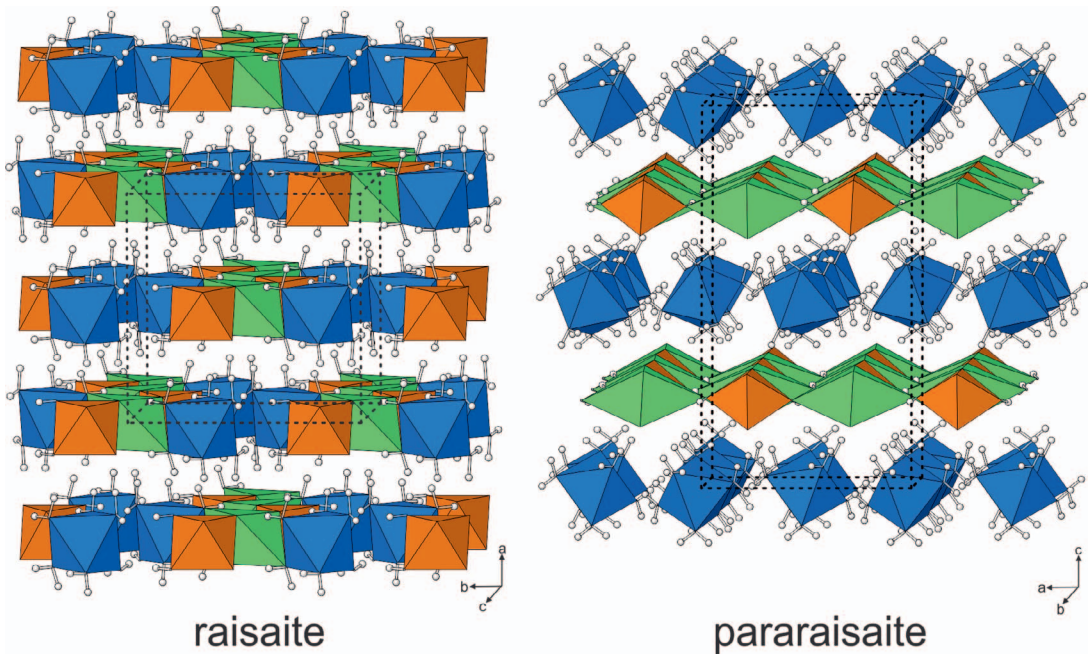

FIG. 5. The crystal structures of raisaite and pararaisaite. Hydrogen bonds are not shown. The unit cell outline is shown with dashed lines.

are given in Table 3, atom coordinates and displacement parameters in Table 4, selected bond distances in Table 5, and a bond valence analysis in Table 6. A CIF file that also contains observed and calculated structure factors has been deposited and is available from the Depository of Unpublished Data on the MAC website[1].

Atomic Arrangement

The structure of pararaisaite contains four different cation sites, Mg1, Mg2, Cu, and Te, all with octahedral coordinations. The $Mg(H_2O)_6$ octahedra are both slightly squat, each with one pair of slightly shorter *cis* Mg–O bonds. The $Te^{6+}O_4(OH)_2$ octahedra are somewhat elongated, with one pair of longer Te–O bonds to *cis* OH groups. The $Cu^{2+}O_4(OH)_2$ octahedra are dramatically elongated, with one pair of much longer Cu–O bonds to *cis* OH groups. This elongation is typical of Cu^{2+} coordinations exhibiting the Jahn-Teller effect.

The $Cu^{2+}O_4(OH)_2$ and $Te^{6+}O_4(OH)_2$ octahedra are linked by sharing *trans* O–O edges to form straight chains of alternating Cu and Te octahedra along [010]. The octahedra in the chains are linked to octahedra in adjacent chains by sharing OH–OH corners yielding a $[Cu^{2+}Te^{6+}O_4(OH)_2]^{2-}$ sheet parallel to {001} (Fig. 4). The $Mg(H_2O)_6$ octahedra, located in the interlayer between $[Cu^{2+}Te^{6+}O_4(OH)_2]$ sheets, are unconnected to one another and to the octahedra in the sheets except by hydrogen bonds (Fig. 5).

The structure of raisaite (Pekov *et al*. 2016), with which pararaisaite is dimorphous, contains the same general types of octahedra; however, they are linked in quite different ways. In raisaite, $Cu^{2+}O_4(H_2O)_2$ and $Te^{6+}O_4(OH)_2$ octahedra share O–O edges; however, the shared edges of the $Te^{6+}O_4(OH)_2$ octahedra are not *trans* and the resulting edge-sharing chain is zig-zag, rather than straight. Furthermore, the $Mg(H_2O)_6$ octahedra in the structure of raisaite are linked directly to the zig-zag chains by sharing two *cis* corners with $Cu^{2+}O_4(H_2O)_2$ octahedra in the same chain (Fig. 4). The complete $[Cu^{2+}MgTe^{6+}O_4(OH)_2(H_2O)_6]$ chains are linked to one another by hydrogen bonds. The hydrogen-bonded chains form layers parallel to {100} and the layers are linked to one another by hydrogen bonds.

In the structural classification of Te oxysalts of Christy *et al*. (2016), pararaisaite falls into the category of structures with "monomeric $Te^{6+}X_6$ as part of a larger structural unit that is an infinite layer". No phase listed in that classification contains a sheet identical to the $[Cu^{2+}Te^{6+}O_4(OH)_2]$ sheet in pararaisaite; however, the recently determined structure of cesbronite, $Cu^{2+}{}_3Te^{6+}O_4(OH)_4$ (Missen *et al*. 2018), contains a very similar sheet. The cesbronite sheet contains edge- and corner-sharing octahedra with the same topology as the sheet in pararaisaite; however, all of these octahedra are identical in cesbronite, being centered by cation sites of occupancy $Cu_{0.5}Te_{0.5}$. As noted by Missen *et al*. (2018), the sheet in cesbronite can be viewed as resulting from the average of two different Cu-Te ordering schemes. In one scheme, edge-sharing chains of all Cu-centered octahedra alternate with chains of all Te-centered octahedra, while the other scheme is identical to that in pararaisaite (Fig. 4).

Acknowledgments

Reviewers Stuart Mills and Andrew Christy are thanked for their constructive comments on the manuscript. At Caltech, the microprobe analyses and Raman studies were funded by grants from the Northern California Mineralogical Association and NSF grant EAR-1322082. The rest of this study was funded by the John Jago Trelawney Endowment to the Mineral Sciences Department of the Natural History Museum of Los Angeles County.

References

Blasse, G. & Hordijk, W. (1972) The vibrational spectrum of Ni_3TeO_6 and Mg_3TeO_6. *Journal of Solid State Chemistry* **5**, 395–397.

Christy, A.G., Mills, S.J., & Kampf, A.R. (2016) A review of the structural architecture of tellurium oxycompounds. *Mineralogical Magazine* **80**, 415–545.

Ferraris, G. & Ivaldi, G. (1988) Bond valence vs. bond length in O···O hydrogen bonds. *Acta Crystallographica* **B44**, 341–344.

Frikha, H., Abdelhedi, M., Mohamed Dammak, M., & Garcia-Granda, S. (2017) Structural single crystal, thermal analysis and vibrational studies of the new rubidium phosphate tellurate $Rb_2HPO_4RbH_2PO_4{\cdot}Te(OH)_6$. *Journal of Saudi Chemical Society* **21**, 324–333.

Gagné, O.C. & Hawthorne, F.C. (2015) Comprehensive derivation of bond-valence parameters for ion pairs involving oxygen. *Acta Crystallographica* **B71**, 562–578.

Higashi, T. (2001) *ABSCOR*. Rigaku Corporation, Tokyo, Japan.

[1] Supplementary Data is available from the Depository of Unpublished data on the MAC website (http://mineralogicalassociation.ca/), document "Pararaisaite, CM56, 18-00044".

KAMPF, A.R., MILLS, S.J., HOUSLEY, R.M., MARTY, J., & THORNE, B. (2010) Lead-tellurium oxysalts from Otto Mountain near Baker, California: V. Timroseite, $Pb_2Cu^{2+}{}_5(Te^{6+}O_6)_2(OH)_2$, and paratimroseite, $Pb_2Cu^{2+}{}_4(Te^{6+}O_6)_2(H_2O)_2$, new minerals with edge-sharing Cu-Te octahedral chains. *American Mineralogist* **95**, 1560–1568.

KAMPF, A.R., MILLS, S.J., HOUSLEY, R.M., ROSSMAN, G.R., MARTY, J., & THORNE, B. (2013) Lead–tellurium oxysalts from Otto Mountain near Baker, California: X. Bairdite, $Pb_2Cu^{2+}{}_4Te^{6+}{}_2O_{10}(OH)_2(SO_4)\cdot H_2O$, a new mineral with thick HCP layers. *American Mineralogist* **97**, 1315–1321.

LINDGREN, W. & LOUGHLIN, G.F. (1919) Geology and Ore Deposits of the Tintic Mining District. United States Geological Survey, Professional Paper **107**, 276 pp.

MANDARINO, J.A. (1976) The Gladstone-Dale relationship – Part 1: derivation of new constants. *Canadian Mineralogist* **14**, 498–502.

MILLS, S.J. & CHRISTY, A.G. (2013) Revised values of the bond valence parameters for Te^{IV}–O, Te^{VI}–O and Te^{IV}–Cl. *Acta Crystallographica* **B69**, 145–149.

MISSEN, O.P., MILLS, S.J., WELCH, M.D., SPRATT, J., RUMSEY, M.S., BIRCH, W.D., & BRUGGER, J. (2018) The crystal structure of cesbronite, $Cu_3TeO_4(OH)_4$: a novel sheet tellurate topology. *Acta Crystallographica* **B74**, 24–31.

PEKOV, I.V., VLASOV, E.A., ZUBKOVA, N.V., YAPASKURT, V.O., CHUKANOV, N.V., BELAKOVSKIY, D.I., LYKOVA, I.S., APLETALIN, A.V., ZOLOTAREV, A.A., & PUSCHCHAROVSKY, D.Y. (2016) Raisaite, $CuMg[Te^{6+}O_4OH)_2]\cdot 6H_2O$, a new mineral from Chukotka, Russia. *European Journal of Mineralogy* **28**, 459–466.

RUMSEY, M.S., WELCH, M.D., MO, F., KLEPPE, A.K., SPRATT, J., KAMPF, A.R., & RAANES, M.P. (2018) Millsite Cu $TeO_3\cdot 2H_2O$: A new polymorph of teineite from Gråurdfjellet, Oppdal kommune, Norway. *Mineralogical Magazine* **82**, 433–444.

SHELDRICK, G.M. (2015a) SHELXT - Integrated space-group and crystal-structure determination. *Acta Crystallographica* **A71**, 3–8.

SHELDRICK, G.M. (2015b) Crystal Structure refinement with *SHELX*. *Acta Crystallographica* **C71**, 3–8.

Received May 9, 2018. Revised manuscript accepted August 8, 2018.